Supplementary Information

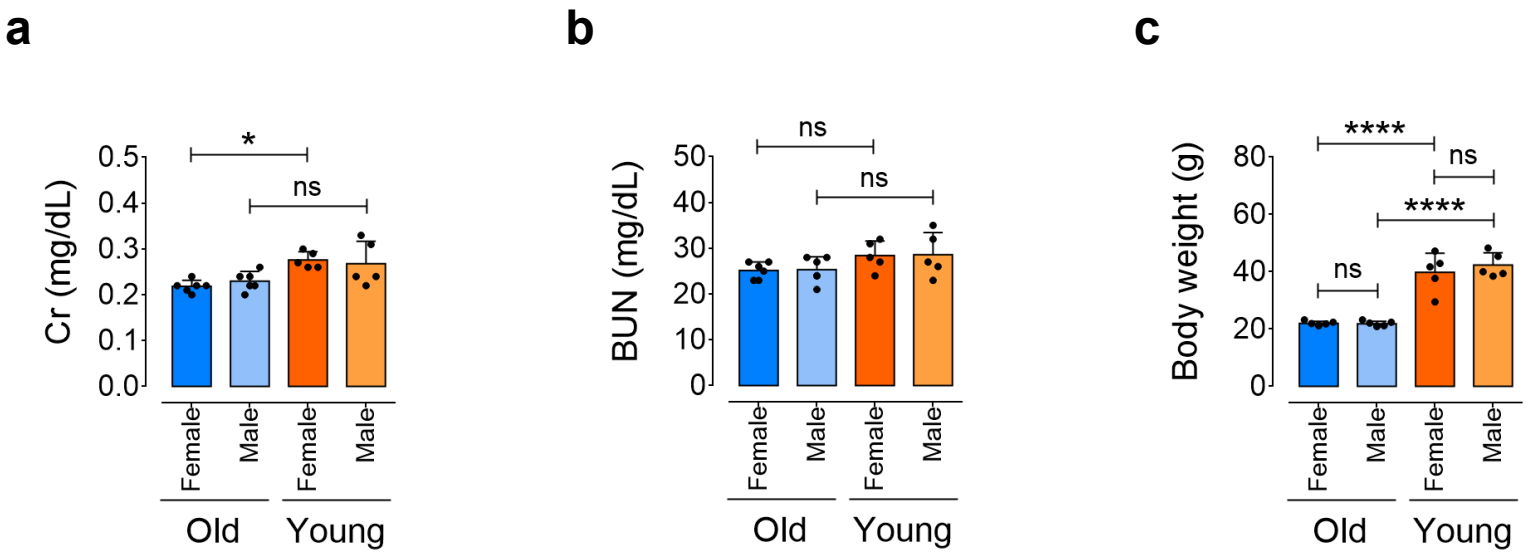

Fig. 1. Kidney function profile in aging. a, Analysis of body weight in female and male, old and young mice (n=5-6). **b,c,** Bar charts showing kidney function profiles, represented as concentrations of creatinine (Cr) (**b**) and BUN (**c**) in sera of female and male, old and young mice (n=5-6). Error bars represent SD (**a-c**). *P* values were calculated using two-way ANOVA followed by Tukey's post *hoc* test (**a-c**). (**P*<0.05, *****P*<0.0001, ns, not significant). Source data are provided as a Source Data file.

a

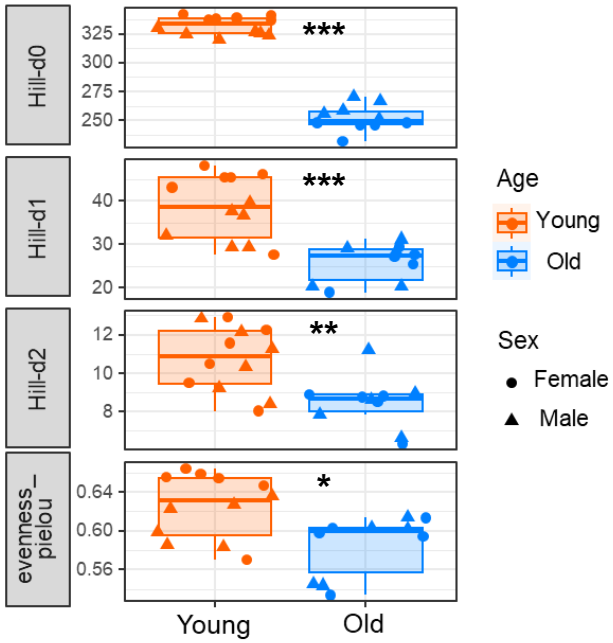
Hill-d0
Hill-d1
Hill-d2
evenness_pielou
***
***
**
*
Young
Old
Age
Young
Old
Sex
Female
Male

b

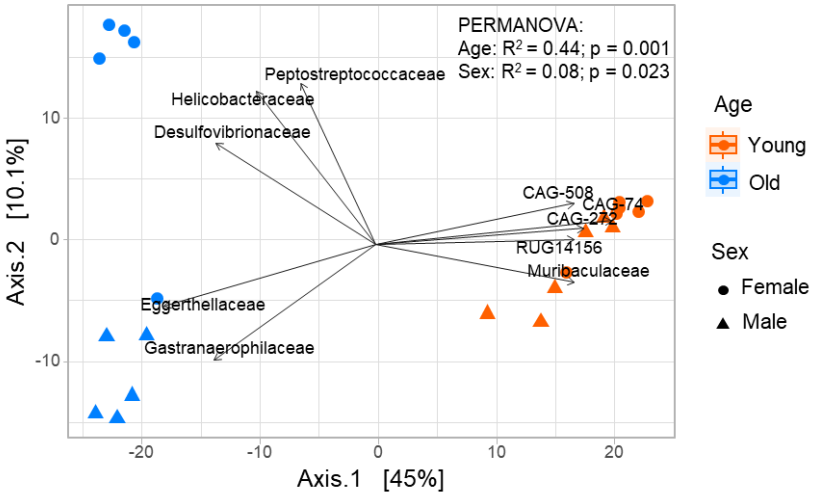
PERMANOVA:
Age: R² = 0.44; p = 0.001
Sex: R² = 0.08; p = 0.023
Peptostreptococcaceae
Helicobacteraceae
Desulfovibrionaceae
CAG-508
CAG-374
CAG-272
RUG14156
Muribaculaceae
Eggerthellaceae
Gastranaerophilaceae
Axis.2 [10.1%]
Axis.1 [45%]
Age
Young
Old
Sex
Female
Male

c

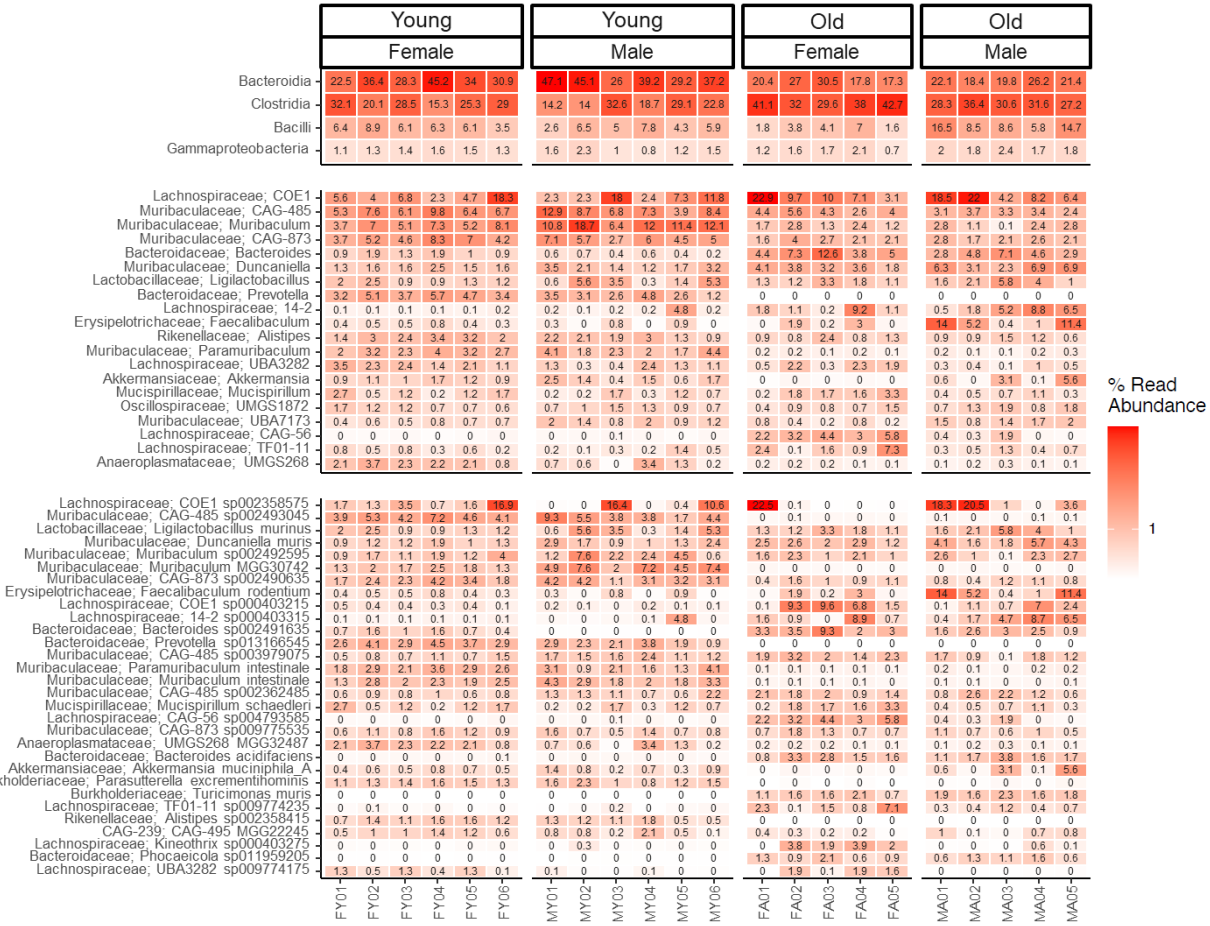
Young Female
Young Male
Old Female
Old Male
Bacteroidia
Clostridia
Bacilli
Gammaproteobacteria
Lachnospiraceae; COE1
Muribaculaceae; CAG-485
Muribaculaceae; Muribaculum
Muribaculaceae; CAG-873
Bacteroidaceae; Bacteroides
Muribaculaceae; Duncaniella
Lactobacillaceae; Ligilactobacillus
Bacteroidaceae; Prevotella
Lachnospiraceae; 14-2
Erysipelotrichaceae; Faecalibaculum
Rikenellaceae; Alistipes
Muribaculaceae; Paramuribaculum
Lachnospiraceae; UBA3282
Akkermansiaceae; Akkermansia
Mucispirillaceae; Mucispirillum
Oscillospiraceae; UMGS1872
Muribaculaceae; UBA7173
Lachnospiraceae; CAG-56
Lachnospiraceae; TF01-11
Anaeroplasmataceae; UMGS268
Lachnospiraceae; COE1 sp002358575
Muribaculaceae; CAG-485 sp002493045
Lactobacillaceae; Ligilactobacillus murinus
Muribaculaceae; Duncaniella muris
Muribaculaceae; Muribaculum sp002492595
Muribaculaceae; Muribaculum MGG30742
Muribaculaceae; CAG-873 sp002490635
Erysipelotrichaceae; Faecalibaculum_rodentium
Lachnospiraceae; COE1 sp000403215
Lachnospiraceae; 14-2 sp000403315
Bacteroidaceae; Bacteroides sp002491635
Bacteroidaceae; Prevotella sp013166545
Muribaculaceae; CAG-485 sp003979075
Muribaculaceae; Paramuribaculum intestinale
Muribaculaceae; Muribaculum intestinale
Muribaculaceae; CAG-485 sp002362485
Mucispirillaceae; Mucispirillum schaedleri
Lachnospiraceae; CAG-56 sp004793585
Muribaculaceae; CAG-873 sp009775535
Anaeroplasmataceae; UMGS268 MGG32487
Bacteroidaceae; Bacteroides acidifaciens
Akkermansiaceae; Akkermansia muciniphila_A
Burkholderiaceae; Parasutterella_excrementihominis
Burkholderiaceae; Turicimonas muris
Lachnospiraceae; TF01-11 sp009774235
Rikenellaceae; Alistipes sp002358415
CAG-239; CAG-495 MGG22245
Lachnospiraceae; Kineothrix sp000403275
Bacteroidaceae; Phocaeicola sp011959205
Lachnospiraceae; UBA3282 sp009774175
FY01 FY02 FY03 FY04 FY05 FY06
MY01 MY02 MY03 MY04 MY05 MY06
FA01 FA02 FA03 FA04 FA05
MA01 MA02 MA03 MA04 MA05
% Read Abundance
1

Fig. 2. Age-associated gut microbiota alterations. a, Box plots representing alpha diversity in feces of both female and male old and young mice measured by Hill-d0 to 2 and Pielou's evenness indices (n=5-6). **b,** Principal coordinate analysis (PCoA) plot showing beta diversity based on the community level changes in old and young mice (n=5-6). **c,** Heatmap depicting differentially abundant microbial profiles at the strain level (each color represents one bacterial taxa) in the fecal microbiota of female and male, old *versus* young mice (n=5-6). Error bars represent SEM (**a,b**). Data were analyzed using Kruskal-Wallis statistical test (**a**) and Atchinson distance and permutational multivariate analysis of variance (PERMANOVA) tests (**b**). (**P*<0.05, ***P*<0.01, ****P*<0.001). Source data are provided as a Source Data file.

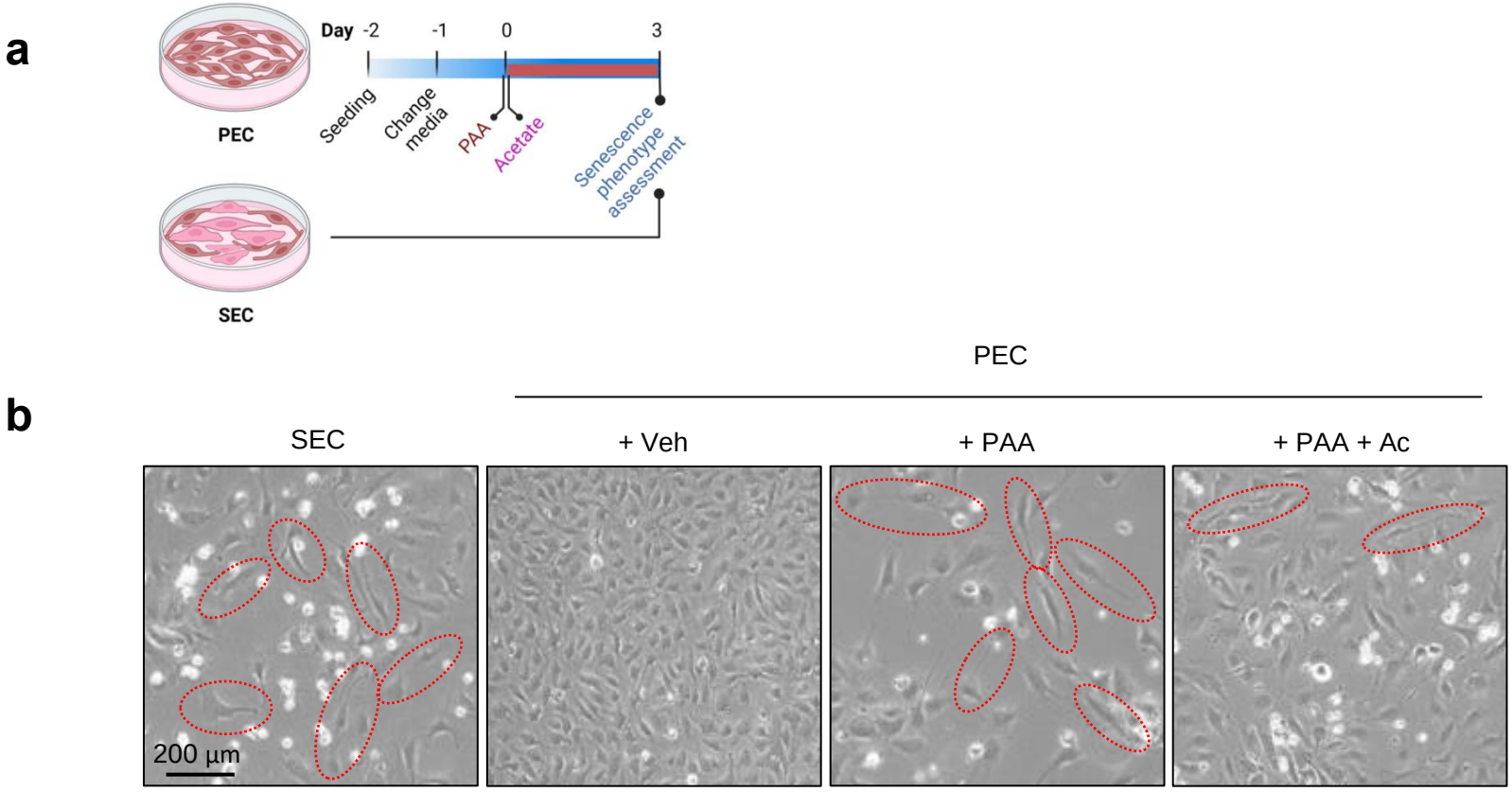

Fig. 3. PAA induces senescence phenotype in endothelial cells. a, Schematic diagram of the experimental setting: SECs, PECs, PAA-treated PECs (10 µM, for 72 h), and PAA+Acetate-treated PECs (PAA: 10 µM, sodium acetate: 3 µM, for 72 h) were assessed for senescence phenotype. **b,** Representative bright-field images depicting cellular senescence-like phenotype, including enlarged, flattened, and multinucleated appearance, in PECs treated with PAA at the magnitude seen in replicative SECs. The images demonstrate that sodium acetate reduces the number of cells with morphologically senescence-like phenotype in PAA-exposed PECs (n=6). Scale bar, 200 µm. Red circles indicate senescent-like cells. Experiments were triplicated independently.

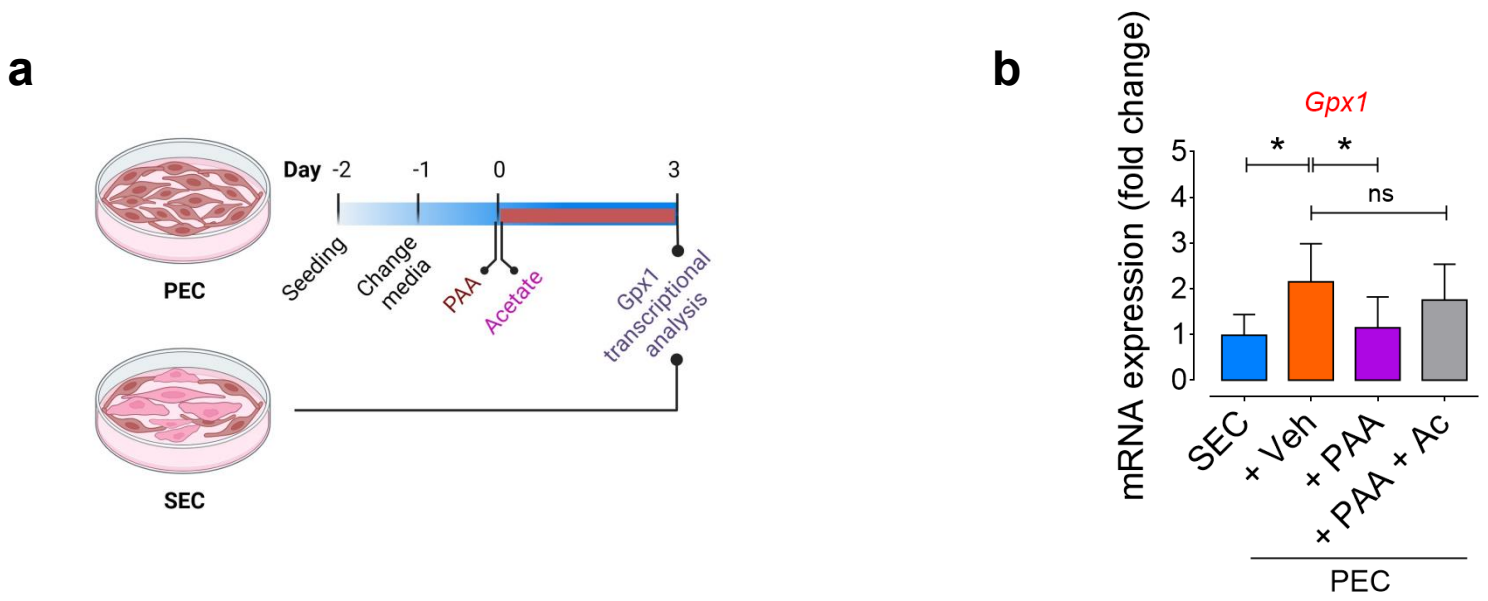

Fig. 4. PAA induces oxidative stress by downregulating antioxidant defense in PECs. a, Schematic diagram of the experimental setting: SECs, PECs, PAA-treated PECs (10 μM, for 72 h), and PAA+Acetate-treated PECs (PAA: 10 μM, sodium acetate: 3 μM, for 72 h) were subjected to glutathione peroxidase 1 (*Gpx1*) transcriptional analysis. **b,** qPCR analysis demonstrating the downregulation of *Gpx1* in PECs in response to PAA and restoration of the gene expression following the addition of sodium acetate (n=6). Error bars represent SD (**a**). Data represent triplicated biologically independent experiments. *P* values were calculated using one-way ANOVA followed by Tukey's post *hoc* test (**a-c**). (**P*<0.05, ns, not significant). Source data are provided as a Source Data file.

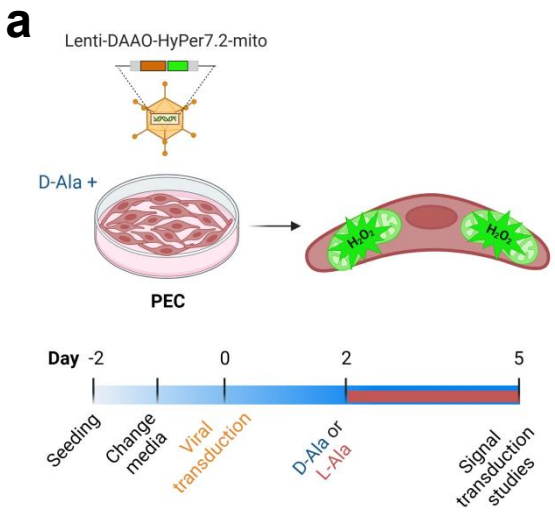
a
Lenti-DAAO-HyPer7.2-mito
D-Ala +
PEC
Day -2
0
2
5
Seeding
Change media
Viral transduction
D-Ala or L-Ala
Signal transduction studies

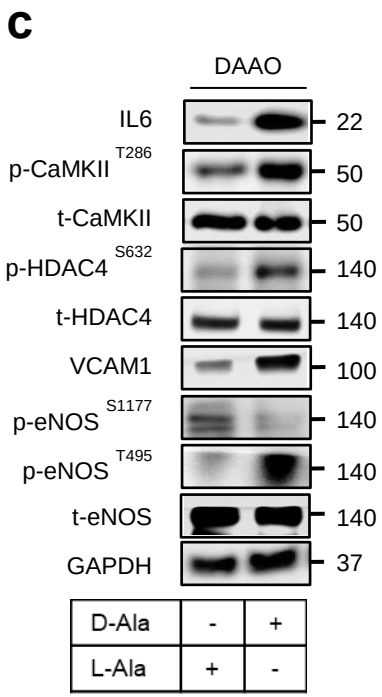
c
DAAO
IL6
p-CaMKII T286
t-CaMKII
p-HDAC4 S632
t-HDAC4
VCAM1
p-eNOS S1177
p-eNOS T495
t-eNOS
GAPDH
22
50
50
140
140
100
140
140
140
37
D-Ala - +
L-Ala + -

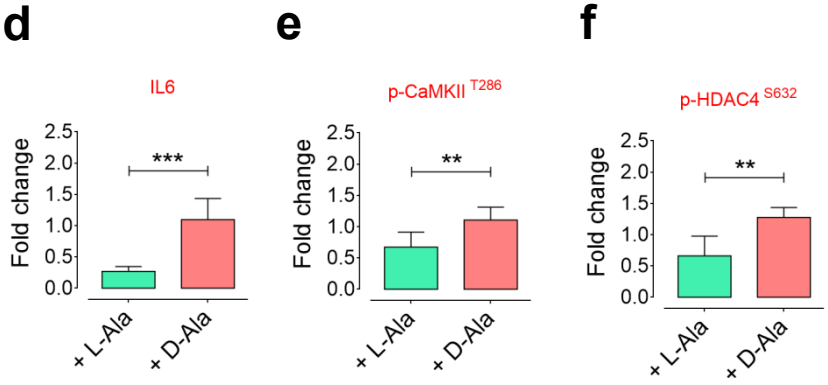
d
IL6
Fold change
***
+ L-Ala
+ D-Ala
e
p-CaMKII T286
**
f
p-HDAC4 S632
**

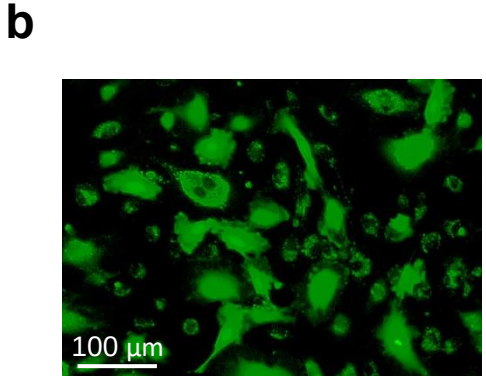
b
100 µm

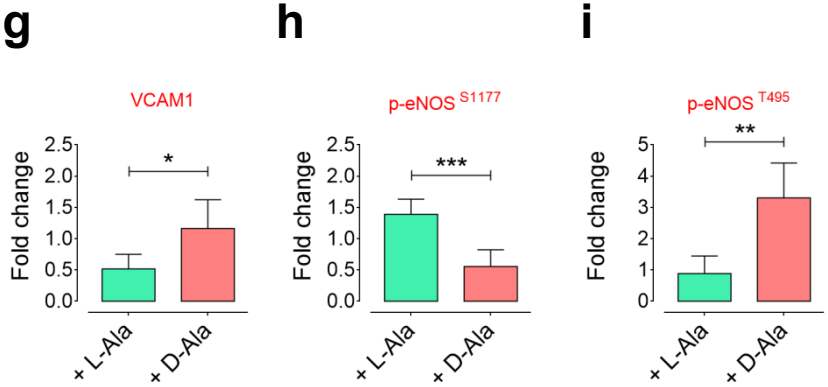
g
VCAM1
Fold change
*
+ L-Ala
+ D-Ala
h
p-eNOS S1177
***
i
p-eNOS T495
**

Fig. 5. Chemogenetic mitochondrial H_2O_2 regulates endothelial NO signaling through IL6-HDAC4 pathway. **a,** Schematic diagram of the experimental setting: PECs were transduced with lentiviral vectors encoding D-aminoacid oxidase (DAAO)-HyPer7.2 targeted to the cell mitochondria for generation of mitochondrial H_2O_2 in the presence D-alanine (10 mM) for 72 h. **b,** Representative widefield ratiometric HyPer7.2 images of PECs transduced with Lenti-DAAO-HyPer7.2-mito constructs. **c-i,** Immunoblots (**c**) and quantitative plots show that chemogenetic mitochondrial H_2O_2, produced by DAAO in response to D-alanine but not L-alanine, orchestrates IL6-mediated CaMKII-HDAC4 phosphorylation and the subsequent VCAM1-regulated eNOS phosphorylation at Ser1177 and Thr495 in PECs (n=6). Scale bar, 100 μm. Error bars represent SD (**d-i**). Data represent triplicated biologically independent experiments. *P* values were calculated using a two-tailed unpaired Student's *t*-test (**d-i**). (**P*<0.05, ***P*<0.01, ****P*<0.001, ns, not significant). Source data are provided as a Source Data file.

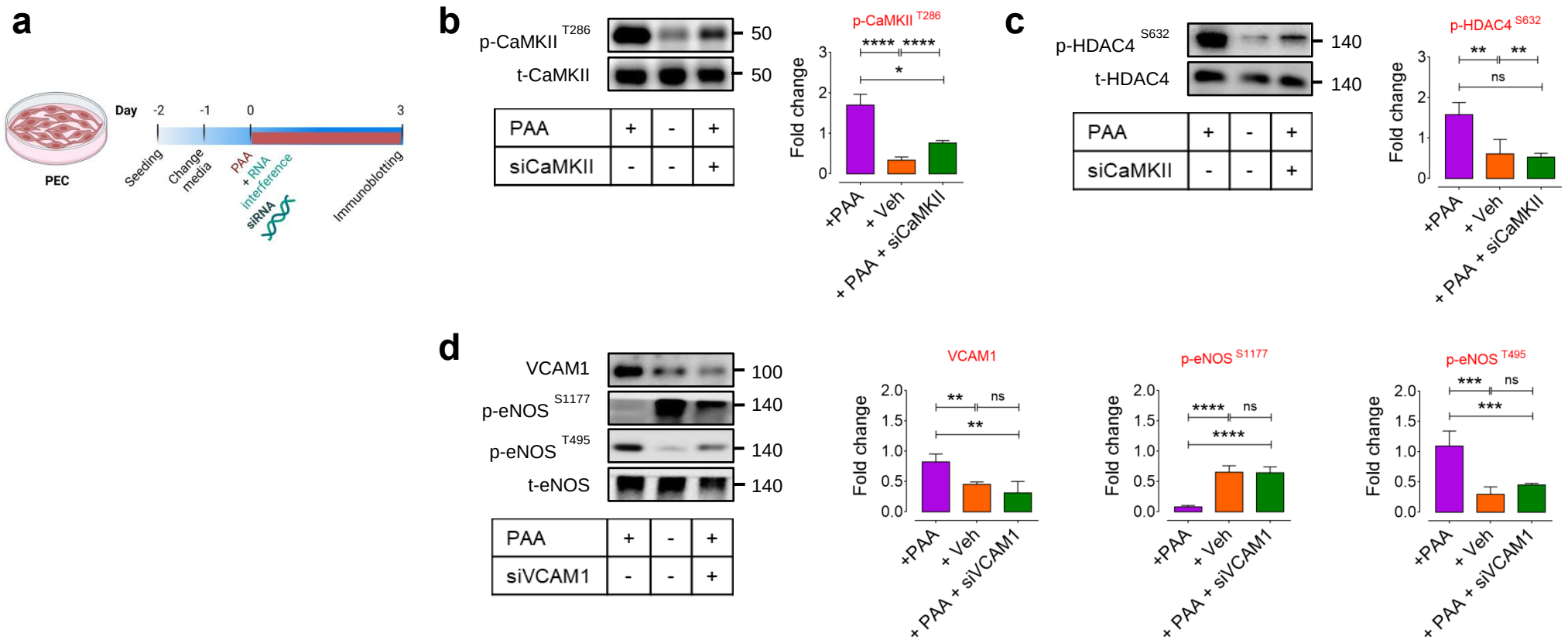

Fig. 6. CaMKII-mediated SASP pathway underlies PAA-induced EC dysfunction. a, Schematic diagram of the experimental setting: PECs were transfected with siCaMKII or siVCAM1 in the presence or absence of PAA (10 μM). **b,c,** Immunoblots (left) and quantitative plots (right) characterizing the effects of PAA on the PAA-induced post-translational modifications of CaMKII (**b**) and its downstream epigenetic regulator HDAC4 (**c**) using CaMKII knockdown approach in PECs (n=6). **d,** Analysis of VCAM1 expression and eNOS phosphorylation at Ser1177 and Thr495 in siVCAM1-transfected PECs in the presence or absence of PAA (n=6). Error bars represent SD (**b-d**). Data represent triplicated biologically independent experiments. *P* values were calculated using one-way ANOVA followed by Tukey's post *hoc* test (**b-d**). (**P*<0.05, ***P*<0.01, ****P*<0.001, *****P*<0.0001). Source data are provided as a Source Data file.

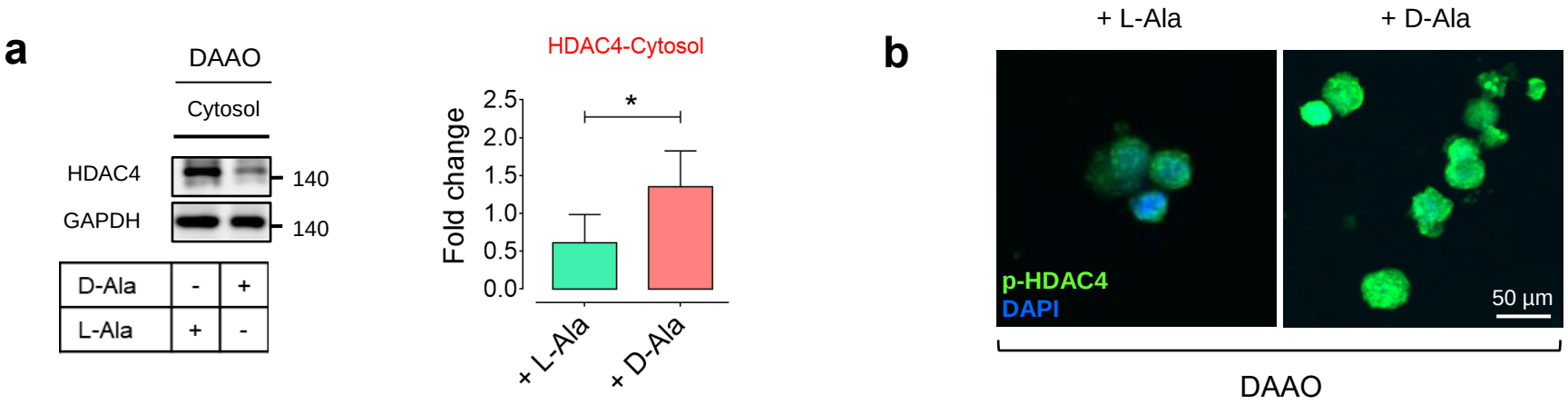

Fig. 7. H_2O_2 orchestrates HDAC4 phosphorylation and its nuclear export. a, Immunoblots (left) and quantitative plot (right) reveal HDAC4 unclear export, represented as an increased expression in the cytosol in response to intracellular H_2O_2 generated by DAAO in the presence of D-alanine (10 mM, for 72 h) in PECs (n=6). **b,** p-HDAC4 immunostaining shows that intracellular H_2O_2 markedly increases HDAC4 phosphorylation that facilitates its translocation towards the cell cytosol in PECs (n=6). Scale bar, 50 µm. Error bars represent SD (**a**). Data represent triplicated biologically independent experiments. *P* values were calculated using a two-tailed unpaired Student's *t*-test (**a**). (**P*<0.05, ***P*<0.01, ****P*<0.001, ns, not significant). Source data are provided as a Source Data file.

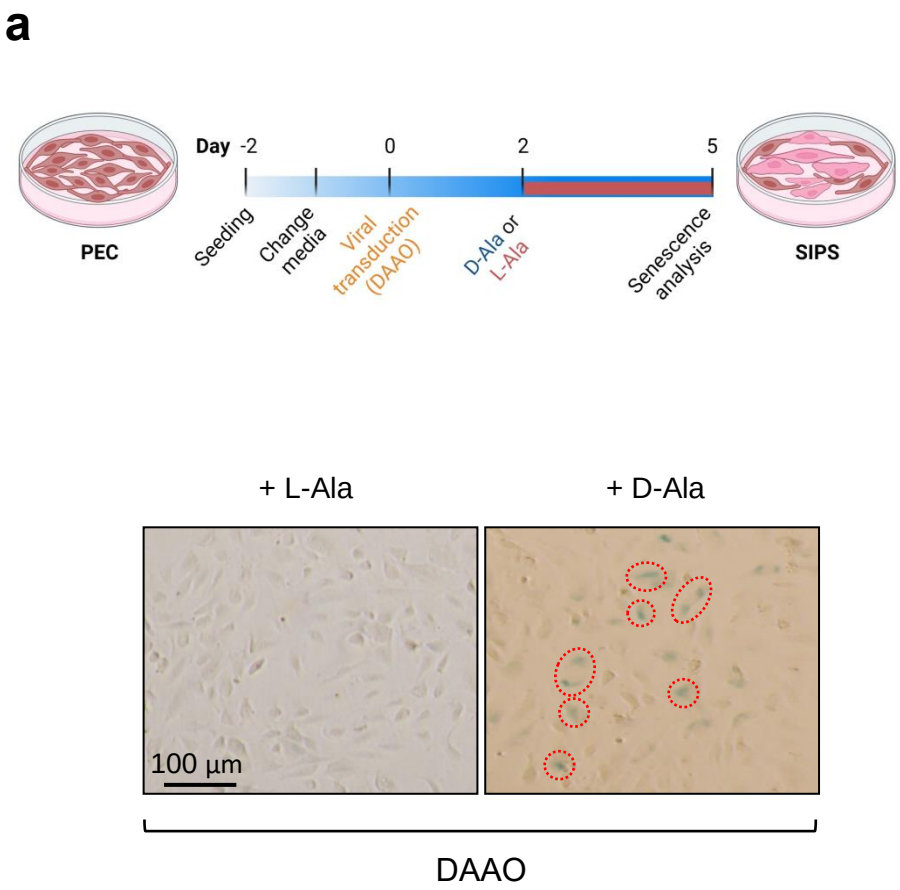
a
PEC
Day -2
0
2
5
Seeding
Change media
Viral transduction (DAAO)
D-Ala or L-Ala
Senescence analysis
SIPS
+ L-Ala
+ D-Ala
100 µm
DAAO
b
DAAO
γ-H2A.X
GAPDH
15
37
L-Ala + -
D-Ala - +
γ-H2A.X
Fold change
2.5
2.0
1.5
1.0
0.5
0.0
**
+ L-Ala
+ D-Ala
c
DAPI
γ-H2A.X
Merge
+ L-Ala
+ D-Ala
20 µm

Fig. 8. Chemogenetic H_2O_2 promotes EC senescence. **a,** Schematic diagram of the experimental setting: PECs were transduced with lentiviral vectors encoding D-aminoacid oxidase (DAAO) targeted to the cell mitochondria for generation of mitochondrial H_2O_2 in the presence D-alanine (10 mM) for 72 h. Representative images of SA-β-gal staining demonstrates that DAAO-mediated mitochondrial H_2O_2 induced cellular senescence in PECs, as shown by increased SA-β-gal-positive cells (%) (n=6). **b,c,** Immunoblots (**b**) and γ-H2A.X immunostaining images (**c**) reveal a marked increase in DDR following mitochondrial H_2O_2 production in DAAO-transduced PECs incubated with D-alanine (n=6). Scale bar, 20 and 100 μm. Red circles indicate SA-β-gal-positive cells. Data represent triplicated biologically independent experiments. Source data are provided as a Source Data file.

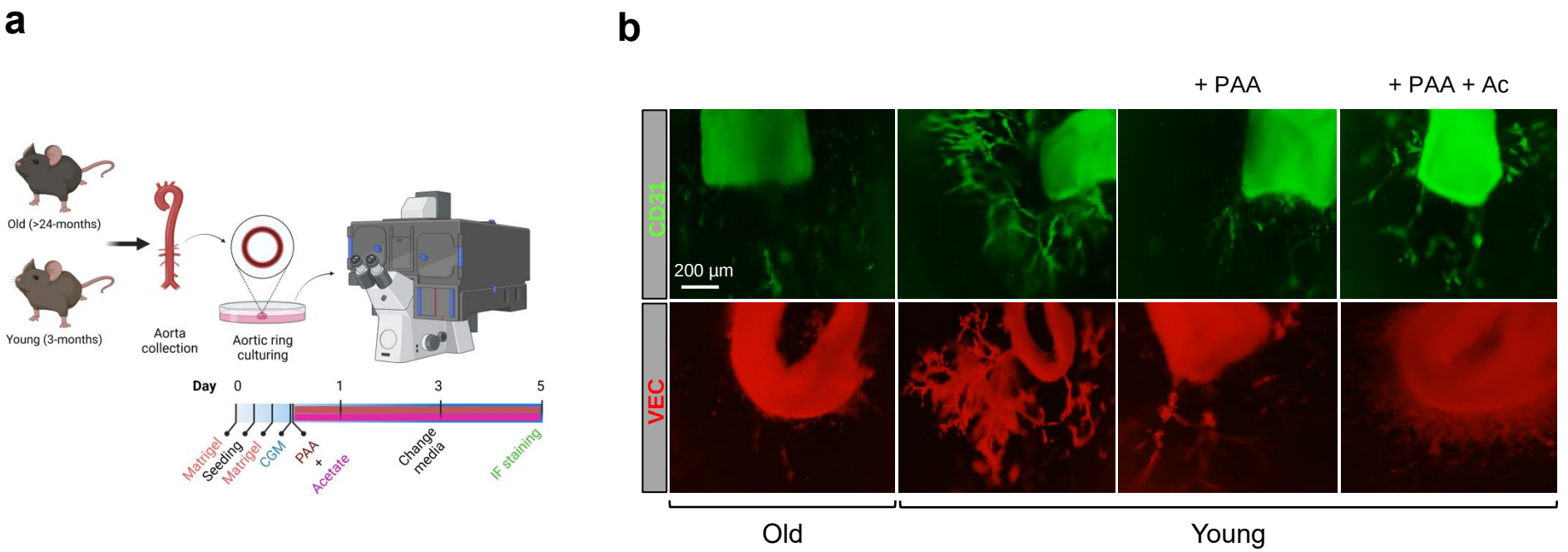

Fig. 9. PAA reduces aortic endothelial sprouting. a, Schematic diagram of the experimental setting: aortic rings from old and young mice were subjected to PAA (10 µM) for 72 h and tested for endothelial sprouting, followed by CD31 (green) and VEC (red) immunofluorescence staining. **b,** CD31 and VEC immunofluorescence staining in mouse aortas showing decreased endothelial sprouting after incubation of young aortic rings with PAA as opposed to vehicle. Immunofluorescence images reveal that co-treatment with sodium acetate markedly restores angiogenic capacity of aortic CD31, VEC-positive ECs (n=6). Scale bar, 200 µm. Experiments were triplicated independently.

Supplementary Table 1. Gene-specific forward and reverse primers for RT-PCR amplification. *Gapdh*, Glyceraldehyde 3-phosphate dehydrogenase; *Gpx1*, Glutathione peroxidase 1; IL1α, Interleukin 1-alpha; *IL1β*, Interleukin 1-beta; *IL6*, Interleukin 6; *p16*, Cdkn2a; *p19*, Cdkn2d; *p21*, Cdkn1a; *Tnfa*, tumor necrosis factor-α; *Vcam1*, Vascular cell adhesion molecule 1.

Gene	**Sequence**	
Gapdh	For: AACAGCAACTCCCACTCTTC	Rev: CCTGTTGCTGTAGCCGTATT
Gpx1	For: CGACATCGAACCTGACATAGAA	Rev: CAGAGTGCAGCCAGTAATCA
IL1α	For: GATACAGAGCACCACAGAGAAC	Rev: GGCTAAGGAAACCCTAGGAAAG
IL1β	For: TCCCAAAGTGCTGGGATTAC	Rev: GAAAGCTCAGAGAGGAGGAAAG
IL6	For: GCCTGCATTAGGAGGTCTTT	Rev: CCTGACACCAGCAAAGGATAA
p16 (Cdkn2a)	For: GGTTCTCGCAGTACCATTGA	Rev: CTGACTTCTGAGGTGGGTTTAG
p19 (Cdkn2d)	For: GTCTCTCCGTTTCCCTTTCTTC	Rev: GCTGGGCGCTTTATTTCATTC
p21 (Cdkn1a)	For: GGGTGCGGTGATGGATAAA	Rev: ACTGCTGAGAACAGGAAGAAC
Tnfa	For: CCCTCGATGAAGCCCAATAAA	Rev: CCCTCCCTCCATTCCTTAGATA
Vcam1	For: CCACTTGCCATCCTACTCTATTC	Rev: CAAGAGGGCTTAGGAGATTAAGG